Ionics (2024) 30:237–246
https://doi.org/10.1007/s11581-023-05281-8

RESEARCH

Design on modified glass fiber separator by ball-milled tin fluoride particles for Zn metal anodes with high reversibility

Huaijun Zhang[1] · Hengyu Yang[1] · Banghui Wu[1] · Yongle Liang[1] · Wentao Ni[1] · Guobao Xu[2] · Liwen Yang[1]

Received: 22 August 2023 / Revised: 18 October 2023 / Accepted: 20 October 2023 / Published online: 6 November 2023

Abstract

Aqueous zinc ion batteries (AZIBs) are considered a promising alternative to lithium-ion batteries for grid-scale energy storage due to superior energy density, high safety, eco-friendliness, and low cost. However, uncontrollable zinc dendrite growth and parasitic side reactions seriously compromise the performance of zinc metal anodes, thereby hindering practical development of AZIBs. In this work, zinc metal anodes are reinforced via a SnF_2-modified glass fiber separator (denoted as SnF_2@GF). Due to excellent ionic conductivity and zincophilicity of SnF_2, the SnF_2@GF separator can effectively homogenize Zn^{2+} flux to inhibit the growth of zinc dendrite and the formation of $Zn_4SO_4(OH)_6{\cdot}5H_2O$ byproducts. As a result, the Zn||Zn symmetric cell exhibits highly reversible plating/stripping behaviors for 1400 h at 1 mA cm^{-2}, and even at 5 mA cm^{-2}, it can operate stably for more than 1000 h. In addition, the assembled Zn||MnO_2 full cells demonstrate a high capacity retention of 80% after 200 cycles at 1 A g^{-1}. Our results provide a facile and low-cost method of enhancing reversibility of zinc metal anodes for high-performance AZIBs.

Keywords Aqueous zinc ion batteries · Zinc anode · Separator modification · Tin fluoride

Introduction

Rechargeable lithium-ion batteries (LIBs) have been widely used in the field of portable and electric vehicles [1]. However, due to expensive lithium resources as well as inherent toxicity and flammability of organic electrolytes, the LIBs suffer from severe cost and safety issues, which limit their application in grid-scale energy storage. In this context, aqueous zinc-ion batteries (AZIBs) with metallic Zn anodes have emerged as promising candidates for large-scale energy storage systems due to competitive energy density as well as high safety, eco-friendliness, and low cost [2–8]. Nevertheless, rough surface of commercial zinc metal anode inevitably leads to uneven distribution of electric field and ion concentration. In these uneven areas, Zn^{2+} ions would preferentially deposit to induce local nucleation and "spike effect," thereby accelerating the formation and growth of zinc dendrites [9]. On the other hand, thermodynamic instability of zinc metal interface and the influence of complex dynamic factors will lead to inevitable and certain degree of hydrogen evolution reaction, which will compete with zinc deposition reaction and reduce the reversibility of zinc electrode. In addition, the continuous hydrogen evolution reaction will lead to the increase of local PH value at the zinc electrode interface, resulting in the formation of passivation byproducts such as $Zn_4SO_4(OH)_6{\cdot}xH_2O$. Therefore, the stability of the interface between zinc anode and aqueous electrolyte is poor owing to the abovementioned dendrite, hydrogen evolution, and passivation reaction, which result in low coulombic efficiency (CE) and unsatisfactory cycle life of AZIBs [10, 11]. It is of great significance to find a suitable strategy to solve the key problems faced by zinc metal anode, thereby achieving high-performance AZIBs [12–15].

Up to now, many strategies have been developed to improve electrochemical performance of zinc metal anode, including artificial interface modification, electrolyte optimization, and separator design [16–26]. Compared to other strategies, separator modification has been shown to be facile and effective to stabilize zinc metal anodes [27–29]. Due to high porosity and wettability, commercial glass fiber (GF) separator is one kind of the most widely used

✉ Liwen Yang
ylwxtu@xtu.edu.cn

[1] School of Physics and Optoelectronics, Xiangtan University, Hunan 411105, China

[2] School of Materials Science and Engineering, Xiangtan University, Hunan 411105, China

separators in the field of AZIBs [30, 31]. However, uneven structure of the larger pores within the commercial GF separator often leads to slow and uneven ion transport, which results in rapid dendrite growth on zinc metal anode to puncture fragile separator and ultimately cause short circuiting of the cell [32–34]. In response to these problems, it was proposed to modify GF separators by suitable functional materials, thereby regulating ion transport and homogenizing zinc deposition to improve the stability of Zn metal anodes [35–39]. Owing to excellent mechanical and electricity properties, carbon-derived materials including vertical graphene, graphene oxide, and graphitic carbon nitride have been used firstly to homogenize zinc deposition and improve the reversibility of Zn metal anodes [40]. Subsequently, other functional materials (for example, Mxene [41], $BaTiO_3$ nanocrystals [42], Sn coating [43], and so on) have also been investigated. Sun et al. [44] prepared a kind of Ti_3C_2Tx MXene-decorated Janus separator by spraying MXene nanosheets on one side of the commercial GF separator. Owing to abundant surface polar groups, good electrolyte wettability, and high ionic conductivity, the Ti_3C_2Tx MXene-decorated Janus separator can facilitate the homogenization of local current distribution and promote nucleation kinetics of zinc, leading to a stable cycling of the assembled symmetric cells for 1200 h at 5 mA cm^{-2}. Very recently, Zhou et al. [45] constructed another kind of Janus separators by spin-coating graphene and sulfonic cellulose on one side of the commercial GF separator and found that it can enable the Zn symmetric cell with a long-term lifespan over 1400 h at 10 mA cm^{-2}/10 mAh cm^{-2} owing to the regulation of Zn growth toward Zn (002) crystallographic orientation and repelling of SO_4^{2-} ions for alleviating side reactions. Despite these fruitful results, the investigation on the modification of the GF separator is still in the initial stage. It is highly desired to modify the GF separators using cheap functional materials that can be produced on large scale.

In this work, ball-milled tin fluoride particles were applied to modify commercial GF separators (denoted as SnF_2@GF) via vacuum filtration, thereby enhancing the reversibility of Zn metal anode. Benefiting from excellent ionic conductivity and high zincophilicity properties of SnF_2, the SnF_2@GF separator can induce a well-distributed Zn^{2+} flux, leading to a uniform deposition of Zn^{2+} on Zn metal anode. The assembled Zn||Zn symmetric cells exhibit stable cycling of more than 1400 h under conventional operating conditions of 1 mA cm^{-2} and 1 mAh cm^{-2}. Meanwhile, the Zn||Cu asymmetric cell equipped with the SnF_2@GF separator operates for more than 300 cycles at 1 mA cm^{-2} with high CE value close to 100%, demonstrating high reversibility of zinc metal anode. In addition, the Zn||MnO_2 full cell exhibits significant cycling stability with 80% capacity retention after 200 cycles at 1 A g^{-1}. The results indicate that the GF separator modified with SnF_2 is an effective method to improve the reversibility of Zn metal anode for high-performance AZIBs.

Experimental

Fabrication of the SnF_2@GF separators

Firstly, commercial SnF_2 powder was ball milled for 10 h to obtain SnF_2 particles with smaller size. Secondly, 12.6 mg ball-milled SnF_2 particles and 1.4 mg poly (vinylidene fluoride) (PVDF, 99.9%, Mw 600,000) were respectively added into 10 ml N-methyl-2-pyrrolidone (NMP, Aladdin, 99.0%), to obtain uniformly mixed solution under ultrasonic treatment for 2 h. Thirdly, ball-milled SnF_2 particles was decorated on GF separator through vacuum filtration of the above mixed solution. Finally, the SnF_2@GF separators were obtained after vacuum drying at 80 °C for 24 h to completely evaporate the NMP solvent. The loading mass of the ball-milled SnF_2 particles can be adjusted by changing the concentration and volume of the SnF_2 and PVDF mixed solution. In detail, the load of 0.5 mg cm^{-2} could be obtained by adding 6.3 mg ball-milled SnF_2 particles and 0.7 mg PVDF into NMP solution, and the load of 2 mg cm^{-2} could be obtained by adding 25 mg ball-milled SnF_2 particles and 2.7 mg PVDF into NMP solution. In addition, the commercial GF separators modified with PVDF (denoted as PVDF@GF) were prepared using the same method without SnF_2.

Material characterizations

The morphologies and microstructures of the sample were observed by scanning electron microscope (SEM, SU5000). Hydrophilic angle tester (HAT, SDC-100) was conducted to study the wettability of the separator after modification. The crystal structure of the sample was confirmed by X-ray diffraction (XRD, Rigaku D/MAX 2500).

Electrochemical measurements

The Zn||Zn symmetric cell, Zn||Cu asymmetric cell, and Zn||MnO_2 full cell were assembled in the atmosphere using CR2025 coin cells. Prior to cell assembly, Zn and Cu foils were cut into discs of 12 mm diameter. The electrolyte was 2.0 M $ZnSO_4$. Before the cathode fabrication, MnO_2 nanorods were obtained according to previously reported preparation process [46]. The MnO_2 cathodes were prepared by coating a paste mixture of 70 wt% MnO_2 nanorods, 20 wt% conductive black, and 10 wt% PVDF on 0.5 mm carbon paper with a mass loading of about 1.0 and 4.0 mg cm^{-2} active materials. Galvanostatic charge/discharge (GCD) cycling tests were performed on a multi-channel battery test system (NEWARE BTS-610). Electrochemical impedance

spectroscopy (EIS) and cyclic voltammetry (CV) were recorded on an electrochemical workstation (CHI660E).

Results and discussion

First of all, Sn has a high redox potential and excellent zincophilicity, so it is a suitable choice for using Sn-based materials to induce zinc deposition [47]. SnF_2 with good ionic conductivity and excellent zincophilicity was considered to modify the GF separator to allow uniform deposition of Zn^{2+} during cycling [48, 49]. The haphazard internal structure of commercial GF separators results in inhomogeneous electric fields and ion channels. The electric field between the diaphragm and the zinc anode can be homogenized by introducing a conductor layer of SnF_2 on the GF separator [50, 51]. Figure 1 a illustrates the fabrication of the SnF_2@GF separator, in which the ball-milled SnF_2 particles and PVDF mixture was vacuum-filtrated into surface and internal pores of the GF separator. Fig. S1a shows an SEM image of commercial SnF_2 with a large particle size and irregular shape, while ball-milled SnF_2 exhibits a smaller particle size and regular shape (Fig. 1b). This helps SnF_2 uniformly fill the pores of the GF separator and deposition on the surface. Inside the GF separators, there are many disorderly fibers with uneven and large holes (Fig. 1c). Through a simple vacuum filtration process, SnF_2 was well filled on the surface of the GF separator and in the cluttered pores inside (Fig. S1b). Compared with the morphology of bare GF, the SnF_2@GF separator has uniform pores and a flat surface with good SnF_2 distribution. Such SnF_2@GF separators have the advantages of optimizing the pore structure for uniform ion transport flux and smoothing the surface of the GF, resulting in well-proportioned Zn^{2+} deposition. Further experiments found that the direct use of SnF_2 caused the separator itself to lose some lubrication because of the larger particles, which were not conducive to the penetration of the electrolyte. Therefore, the ball-milled SnF_2 was pumped onto the separator by vacuum filtration (Fig. 1d), and the SEM image showed that the inside of the separator was somewhat filled but not clogged, resulting in good wettability. The digital image of pristine SnF_2@GF separator (wet and white) and GF (pure white) can be observed that uniform color distributed over the whole sample (Fig. S1c).

The XRD pattern of SnF_2@GF shows characteristic peaks of 25.3°, 26.6°, 28.1°, and 28.5°, which correspond to SnF_2, respectively (Figure S2, Supporting Information), suggesting that SnF_2 is successfully introduced onto the GF surface. In order to investigate the effect of SnF_2 decoration on ion transport, the ionic conductivity of the separator was determined using electrochemical impedance spectroscopy (EIS). As shown in Figure S3, the ionic conductivity of SnF_2@GF was 67.6 mS cm^{-2}, which is much higher than that of the blank GF (29.7 mS cm^{-2}), indicating that faster ion diffusion can be achieved with the SnF_2@GF separator. This faster Zn^{2+} transport capacity brought about by SnF_2

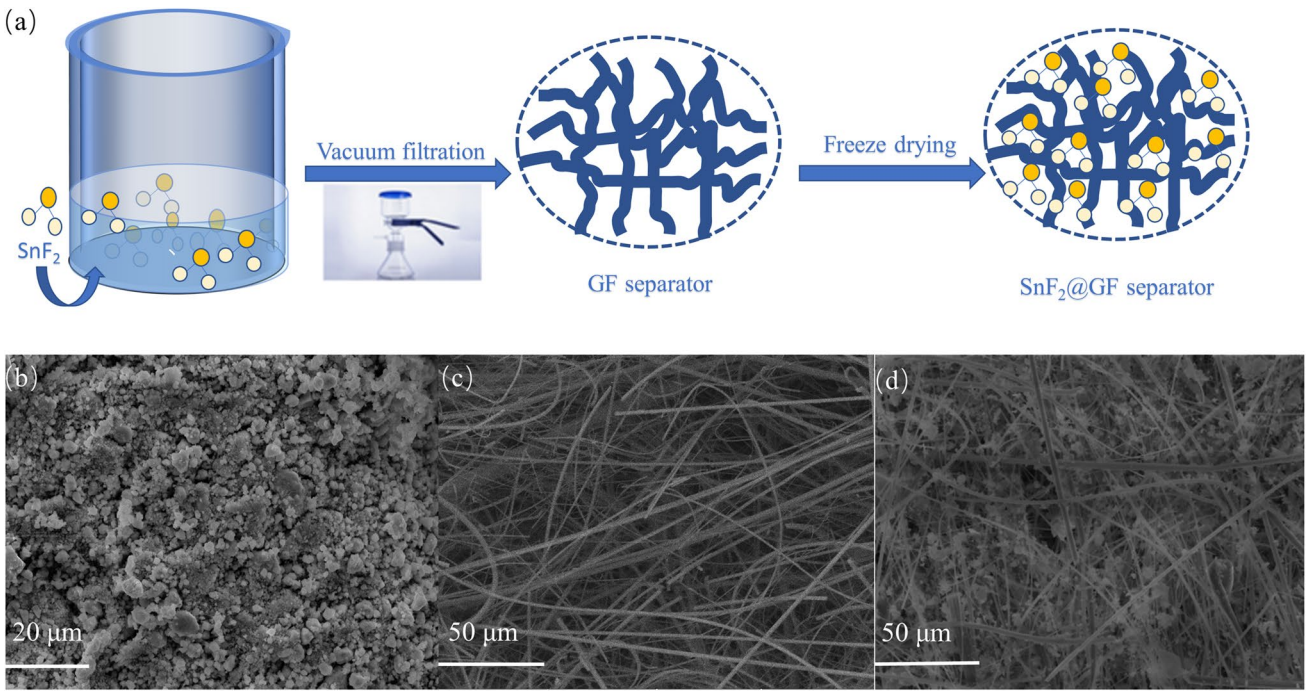

Fig. 1 **a** Schematic illustration of the preparation of SnF_2@GF separator; **b** SEM image of SnF_2 nanoparticles obtained after 10 h of ball milling; **c** SEM images of commercial GF separator; **d** SEM images of SnF_2@GF separator after ball milling

also correlates with the electrolyte wettability of SnF_2@GF, which is as good as that of GF, but more significantly due to the change in surface electrochemical properties. It can be seen that the Zn^{2+} transfer number of the SnF_2@GF separator increases significantly from 0.16 to 0.48 (Fig. S4). Together, the enhanced ionic conductivity and Zn^{2+} transfer number illustrate the improved ion transport kinetics of the SnF_2@GF separation system.

In order to explore the role of such SnF_2@GF separators in improving electrochemical performance of Zn metal batteries, Fig. S5 compares the plating/stripping behavior of Zn||Zn symmetric cells assembled with modified separators of different SnF_2 contents at 1 mA cm^{-2} and 1 mAh cm^{-2} operating conditions, respectively. Clearly, the cell without modification shows larger voltage fluctuations and quickly short circuit after cycling within 200 h. Note that the cyclic stability and polarization effect of Zn plating/stripping can be significantly improved after adopting the SnF_2 separator, although both lower (0.5 mg cm^{-2}) and higher loading contents (2 mg cm^{-2}) in the separator engineering can improve the stability of zinc plating/stripping. Figure S6 compares the SEM results of the SnF_2@GF separators with different loadings, which indicates that either insufficient or excessive filling of the separator surface with SnF_2 leads to inhomogeneous ion transport. At the same time, we compared the mass changes of differently loaded SnF_2@GF separators after immersing them in 2 M $ZnSO_4$ electrolyte for 2 h and calculated their electrolyte uptake (see Fig. S7). SnF_2@GF separators increase the electrolyte absorption with the increase in SnF_2 loading, but when the loading reaches to 2 mg cm^{-2}, the electrolyte absorption is decreasing instead. The above results indicate that the SnF_2@GF separators with 1 mg cm^{-2} loading have the best electrolyte retention capability. The comparative analysis of the results revealed that the cell assembled with separators loaded with 1 mg cm^{-2} had the longest cycle life. Therefore, all the following discussions of the SnF_2@GF separator refer to this optimized content, but not specifically to it. In the hydrophilic angle tester (HAT), significant wetting behavior of the separator was observed for both modified and unmodified SnF_2 (Fig. S8). The SnF_2@GF separators have good wettability, which leads to satisfactory electrolyte storage rates and ion conductivity. Cycling tests were conducted on Zn||Zn symmetric batteries to evaluate protective effect of SnF_2@GF separators on the reversibility of zinc metal anodes by comparing galvanic stability. As shown in Fig. 2 a, with a capacity of 1 mAh cm^{-2}, the SnF_2@GF separator has a stable Zn plating/stripping voltage profile of 1400 h

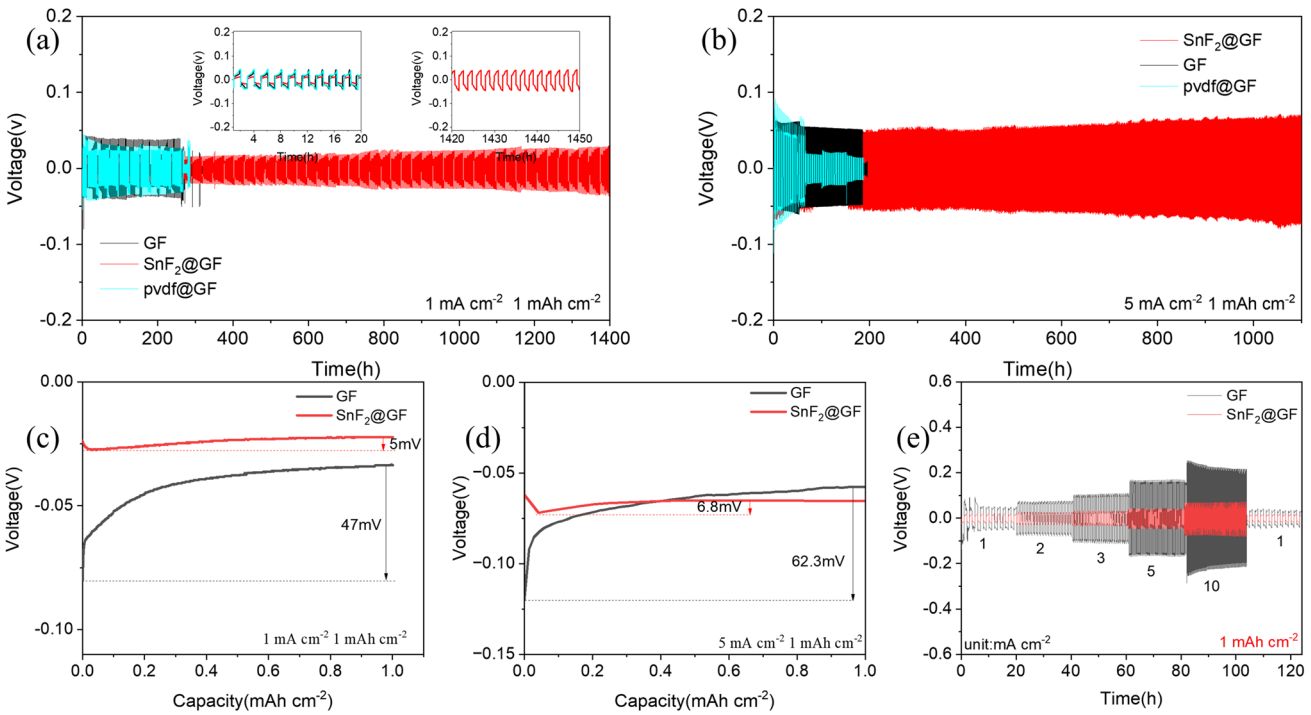

Fig. 2 The cycling performance of Zn||Zn symmetric cells with SnF_2@GF and GF separators at the density and areal capacity of 1 mA cm^{-2}, 1 mAh cm^{-2}; the inset of **a** compares their polarization voltage; **b** the cycling performance of Zn||Zn symmetric cells with SnF_2@GF and GF separators at the density and areal capacity of 5 mA cm^{-2}, 1 mAh cm^{-2}; **c** the corresponding nucleation overpotential of Zn||Zn symmetric cell at 1 mA cm^{-2}, 1 mAh cm^{-2}; **d** the corresponding nucleation overpotential of Zn||Zn symmetric cell at 5 mA cm^{-2}, 1 mAh cm^{-2}; **e** rate performances of Zn||Zn symmetric cells with SnF_2@GF and GF separators at current densities of 1 to 10 mA cm^{-2} and the areal charge capacity of 1 mAh cm^{-2}

and a current density of 1 mA cm^{-2}, which is longer than that of the bare GF (200 h) and PVDF@GF (200 h) separators, indicating improved reversibility of Zn deposition. The magnitude of polarization voltage and the range of rise and fall can evaluate the kinetics and reversibility of Zn deposition. Surprisingly, the cell with SnF_2@GF separator showed the lowest voltage hysteresis of 25 mV compared to the cell with GF (50 mV) and PVDF@GF (50 mV) (Fig. 2a). This indicates that the SnF_2@GF separator successfully inhibits the production of by-products. In this regard, the Zn deposition process can be divided into two parts: the nucleation process of Zn^{2+} and the growth of nucleus [52, 53]. In the initial nucleation stage, Zn^{2+} is required to overcome the nucleation potential barriers corresponding to the nucleation over-potential sites [54]. At the same time, Fig. 2 c shows that the initial relevant nucleation overpotential of cells in the SnF_2@GF separator was only 5 mV at 1 mA cm^{-2}, while the value of cells in the GF separator reached 47 mV. The results show that the SnF_2@GF separator induces a uniformly distributed Zn^{2+} flux, leading to homogeneous zinc deposition with lower energy barriers for zinc nucleation and dissolution in the phase transition between Zn^{2+} and zinc metal, thus suppressing localized accumulation and partial overgrowth phenomena. Surprisingly, the symmetrical battery has a cycle life of more than 1000 h (Fig. 2b), even under high current conditions of 5 mA cm^{-2} and 1 mAh cm^{-2}, far more than the cycle life of the GF separator (180 h). The related voltage hysteresis of cell with GF rises up to 62.3 mV, but that of SnF_2@GF separator only rises up to 6.8 mV (Fig. 2d). Although high current density limits ion transmission, batteries with SnF_2@GF separators still offer remarkable cycle performance and minimal voltage polarization. Based on the consideration of the large current effect, Fig. 2 e compares the speed performance of 1mAh cm^{-2} at different current densities of 1~10 mA cm^{-2} and then returns to the rate performance at 1 mA cm^{-2}. The results showed that the polarization voltage of the symmetrical battery assembled with the ordinary GF separator increased significantly as the current density increased, in contrast to the fact that the polarization voltage in the battery mounted with the SnF_2@GF separator was more stable and far smaller than in ordinary batteries under the same conditions. Therefore, the SnF_2@GF separator not only reduces the generalized nuclear barrier of zinc anodes to form uniform zinc but also promotes the low-polarization effect and improves the zinc sedimentation dynamics. In addition, batteries with SnF_2@ GF separators are superior in current density and cycle time to most other modified separators and zinc anodes (Table S1). Coulombic efficiency (CE) is a key factor in evaluating the stability of the electrodes during the repeated plating/stripping processes. By assembling the GF separators and the SnF_2@GF separators Zn||Cu asymmetric cells, the CE cycle is carried out at a current density of 1 mA cm^{-2} and a surface capacity of 0.5 mAh cm^{-2}. Compared to batteries assembled with ordinary GF separator, the cycle performance and cycle life of batteries mounted with SnF_2@GF separators are significantly improved (Fig. 3a). The GF separators showed a higher nucleation over-potential of 44.6 mV, while the fabrication of the SnF_2@GF separators showed a lower nucleation over-potential value (~22.6 mV) thanks to the high zincophilicity of SnF_2. Moreover, the CE value of the SnF_2@GF separators assembled cell remained close to 100% for 300 cycles at a current density of 1 mA cm^{-2} (Fig. 3b), while the GF separators assembled cell exhibited poor cycle life and lower coulomb efficiency due to the prominent galvanized reversibility provided by the SnF_2@ GF separators to the cell. The above results show that the SnF_2@GF separators not only has excellent zincophilicity properties but also effectively improves the reversibility of plating/stripping and enhances the deposition kinetics, resulting in an ultra-stable zinc metal anode. As shown in Fig. 3 c–d, a mechanism to improve the reversibility of Zn metal anodes using SnF_2@GF separators is proposed. The SnF_2@GF separators with excellent ionic conductivity and zinc affinity homogenizes the electric field between the separator and the zinc anode, and the excellent zinc affinity facilitates the production of a uniform Zn^{2+} flux under a uniform electric field, which leads to the uniform deposition of zinc on the anode. Moreover, the F^- rich in SnF_2 preferentially bind to Zn^{2+} rather than SO_4^{2-}, thus inhibiting the generation of by-products [39]. Therefore, the reversibility of Zn metal anodes can be significantly improved by using SnF_2@ GF separators. For the GF separators, due to the disorderly porous structure inside the separator, Zn^{2+} cannot be uniformly deposited. Moreover, the presence of some uneven areas on the surface and edges of the zinc anode results in uneven electric field distribution, and Zn^{2+} deposition preferentially deposits these uneven areas, resulting in the protrusion. With the increase in cycle time, these protrusions will form zinc crystals, and the growing zinc filament will penetrate the membrane, causing short circuit failure of the battery. Besides, Zn^{2+} will have some side reactions with the electrolyte, generating some insoluble zinc oxides, such as alkaline zinc sulfate. These by-products will not only corrode the zinc anode but will also cause hydrogenation to cover the surface of the zinc anode, preventing the transmission of the discharge products and Zn^{2+} and also causing battery failure. Accordingly, the zinc deposition on the zinc anode with bare GF and SnF_2@GF separators was investigated using ex situ XRD (Fig. 4a). The XRD patterns for the zinc anode with a normal GF separator have distinct diffraction peaks at 8.18°, 16.22°, and 24.43°, which correspond to the characteristic peaks of the byproduct alkaline zinc sulfate ($Zn_4SO_4(OH)_6{\cdot}5H_2O$, PDF No. 39-0688), while the zinc anode based on SnF_2@GF separator has only weak peaks present, proving that the SnF_2@GF separator has a good

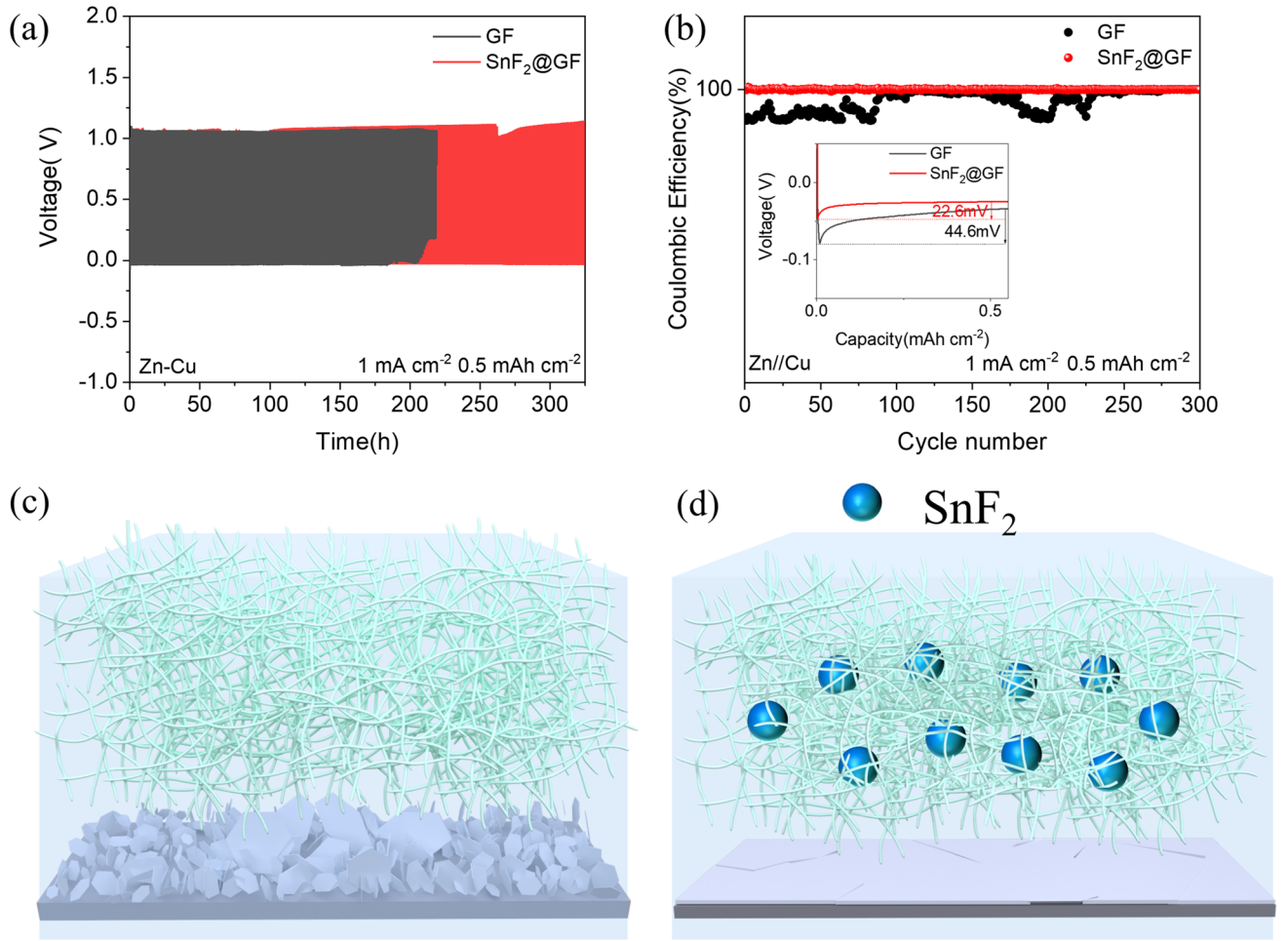

Fig. 3 **a** The cycling performance of Zn||Cu asymmetric cells assembled with SnF_2@GF and GF at the current density of 1 mA cm^{-2} (0.5 mAh cm^{-2}); **b** the corresponding CE of Zn plating/stripping behavior; the inset represents nucleation over¯potential at 1 mA cm^{-2}; **c**, **d** schematic illustration showing the modification and growth of the dendrite process for the SnF_2@GF separator, compared to the GF separator

inhibitory effect on the generation of by-products and dendrites during the cell cycling process. The morphology of the Zn metal anode surface after symmetric cell cycling was characterized by SEM to show the effect of SnF_2@GF separator on the uniform deposition of Zn. Fig. S9 describes the original zinc anode with a smooth surface with polished scratches. As shown in Fig. 4 b, the battery assembled with a commercial GF separator shows obvious dendrites and passivation behavior on the zinc anode after 60 h of cycling, and some areas are covered by a large number of by-products. The uneven galvanized layer intensifies the unevenness of its electric field distribution and ion concentration and also gradually accelerates the consumption of electrolyte, the growth of dendrites, and the formation of by-products. In contrast, a flat and dense zinc deposition layer was detected on the surface of the zinc anode of the cell assembled with SnF_2@GF separator at the same time of cycling (shown in Fig. 4c). Figure S10a shows a cross-sectional SEM image of a zinc-metal anode using the GF separator, showing inhomogeneous and loose features. In contrast, the cross-sectional SEM image of the zinc metal anode using the SnF_2@GF separator exhibits a uniform and compact zinc coating (Figure S10b). EIS can reveal the evolution of interfacial transport kinetics during zinc deposition, where enhanced charge transfer kinetics can promote Zn^{2+} transport. As shown in Fig. 4 d–e, the results indicate that the impedance of the cell with the application of a SnF_2@GF separator is significantly smaller than that of the cell with a normal separator (Table S2, supporting information), which is caused by the reduction of by-products during the cell cycling process on the one hand; on the other hand, it is caused by the good ionic conductivity and excellent zincophilicity of SnF_2 itself. Therefore, the SnF_2@GF separator can promote the transport of Zn^{2+}, achieving a synergistic effect of improved ion transport and uniform Zn deposition.

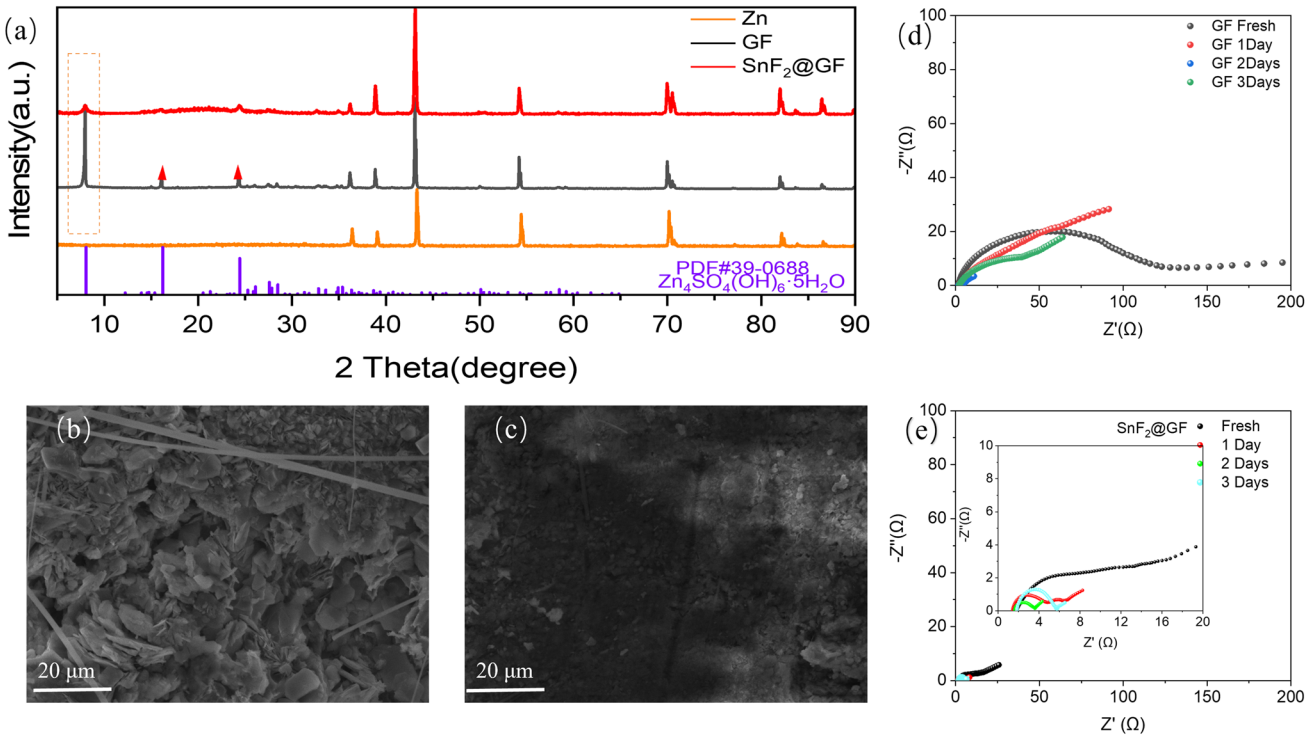

Fig. 4 **a** XRD patterns of cycled zinc metal anodes after cycling for 60 h at the working condition of 1 mA cm^{-2} and 1 mAh cm^{-2}; **b** the corresponding SEM images of cycled Zn anodes with GF and **c** with SnF_2@GF separator; **d** electrochemical impedance spectroscopy measurement of Zn||Zn symmetric cells assembled with GF at different cycles and **e** with SnF_2@GF separator

In order to further evaluate the practical application of the separator modification to enhance the reversibility of Zn metal anodes, the electrochemical performance of Zn||MnO_2 full cells equipped with SnF_2@GF and GF separators was tested. The XRD pattern (Fig. S11) shows that the crystallization of the MnO_2 active material corresponds to α-MnO_2 (JCPDS: 44-0141). As shown in Fig. 5 a, cells with SnF_2@GF separators show less voltage polarization, faster storage dynamics, and greater area capacity when their CV curves are compared to those of unchanged cells in the voltage window of 1.0–1.8 V. To demonstrate that higher electrochemical performance can be achieved for the whole Zn||MnO_2 cells based on the SnF_2@GF separator, the multiplicity performance and capacity retention of the cells before and after the modification of the separator are described in Fig. 5 b–c, respectively. In particular, the battery after the separator can provide a comparative capacity of 84 mAh g^{-1} under 3 A g^{-1}, equivalent to 53.5% of the capacity obtained under 0.2 A g^{-1}. Unmodified ordinary batteries, however, have only 46 mAh g^{-1} capacity and a capacity retention rate of 32.3%. More importantly, the relative capacity of the cell with the SnF_2@GF separator can be restored to 179 mAh g^{-1} and 112.5% retention when the additional current density is restored to 0.2 A g^{-1}. Please note that a retention of more than 100% capacity can be attributed to the gradual activation process of the MnO_2 cathode or the evolution of the storage mechanism. And batteries assembled using GF separators have only 132 mAh g^{-1} capacity and a 91% capacity retention rate when recovering to 0.2 A g^{-1}. In addition, ZIBs based on SnF_2@GF separators were distributed along a discharge curve of 0.2 to 3 A g^{-1} under different current densities, as illustrated in Fig. 5 d. The two platforms on the charging curve are consistent with the oxidation restoration peak on the CV curve, and even under the large current density of 3 A g^{-1}, the second discharge platform can still be observed. Besides that, the charging and discharging curves at different current densities (Fig. S12) confirm the voltage polarization reduction and better redox platform of the cells using SnF_2@GF separators. Additionally, the SnF_2@GF separators make the entire Zn||MnO_2 battery charge transfer resistance much smaller in EIS measurements than the ordinary battery using the GF separator (Fig. 5e). This demonstrated that the SnF_2@GF separator enhanced the transfer kinetics of Zn^{2+}, implying that the interfacial properties and charge transfer kinetics were improved. The cell with SnF_2@GF separator delivers a pristine capacity of 160 mAh g^{-1} over 200 cycles with 80% capacity retention at high current density of 1 A g^{-1}, which is superior to that of 140 mAh g^{-1} with only 32.9% retention for the cell with GF (Fig. 5f). Even at a high loading of 4 mg cm^{-2}, the full cell

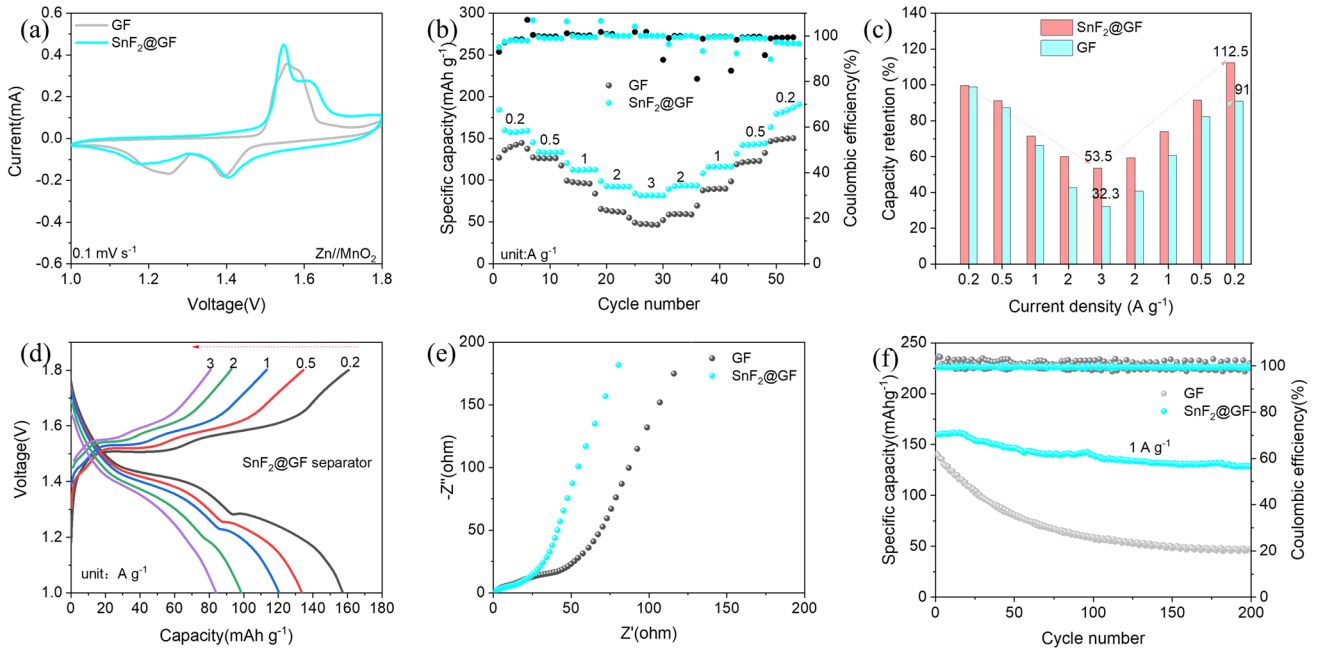

Fig. 5 The electrochemical performance of Zn||MnO_2 full batteries equipped with SnF_2@GF and GF separator. **a** The comparison of CV curve at the scan rate of 0.1 mV s^{-1}; **b** rate performance recorded at various current densities; **c** the corresponding capacity retention comparison; **d** the corresponding charge/discharge curves of SnF_2@GF separators recorded at different current densities; **e** EIS measurement in the initial state before cycle; **f** cycle stability tests at the current density of 1 A g^{-1}

with SnF_2@GF separators still has a high capacity and good stability (see Figure S13).

Conclusions

In conclusion, thanks to excellent ionic conductivity and high zincophilicity of the ball-milled SnF_2 particles, the SnF_2@GF separator induces homogeneous Zn^{2+} deposition to suppress zinc dendrites and by-products, thereby improving the reversibility of Zn metal anode. The Zn||Zn symmetric cells with the SnF_2@GF separators have an ultra-stable cycling performance at 1 mA cm^{-2} for more than 1400 h of operation. Meanwhile, the Zn||Cu asymmetric cell equipped with the SnF_2@GF separator maintains the CE of nearly 100% after 300 cycles at 1 mA cm^{-2}, demonstrating high reversibility of the Zn metal anode. In addition, Zn||MnO_2 full cells equipped with SnF_2@GF separators exhibited remarkable cycling stability with 80% capacity retention after 200 cycles at 1 A g^{-1}. Our results provide a simple, effective, and low-cost strategy of separator modification to enhance the reversibility of zinc metal anodes for high-performance AZIBs.

CRediT authorship contribution Huaijun Zhang: investigation, experimental operation, data curation, writing—original draft. Hengyu Yang: investigation, formal analysis. Banghui Wu: writing—review and editing. Yongle Liang: writing—review and editing, Validation. Wentao Ni: writing—review and editing. Guobao Xu: writing—review and editing. Liwen Yang: supervision, data curation, conceptualization, writing—review and editing.

Supplementary Information The online version contains supplementary material available at https://doi.org/10.1007/s11581-023-05281-8.

Funding This work is financially supported by The National Natural Science Foundation of China (Grant Nos. 12074327, 12002294 and 11774298), The Science and Technology Innovation Program of Hunan Province (No. JJ4088), and Innovation-Driven Project of Xiangtan University (CX 20190471).

Data availability Data will be made available on request.

Declarations

Competing interests The authors declare no competing interests.

References

1. He W, Guo W, Wu H, Lin L, Liu Q, Han X, Xie Q, Liu P, Zheng H, Wang L, Yu X, Peng DL (2021) Challenges and recent advances in high capacity Li-rich cathode materials for high energy density lithium-ion batteries. Adv Mater 33(50):2005937. https://doi.org/10.1002/adma.202005937

2. Wu TH, Zhang Y, Althouse ZD, Liu N (2019) Nanoscale design of zinc anodes for high-energy aqueous rechargeable batteries. Materials Today Nano 6:100032. https://doi.org/10.1016/j.mtnano.2019.100032
3. Blanc LE, Kundu D, Nazar LF (2020) Scientific challenges for the implementation of Zn-Ion batteries. Joule 4(4):771–799. https://doi.org/10.1016/j.joule.2020.03.002
4. Chao D, Zhou W, Xie F, Ye C, Li H, Jaroniec M, Qiao SZ (2020) Roadmap for advanced aqueous batteries: from design of materials to applications. Sci Adv 6(21):aba4098. https://doi.org/10.1126/sciadv.aba4098
5. Liang YL, Dong H, Aurbach D, Yao Y (2020) Current status and future directions of multivalent metal-ion batteries. Nat Energy 5(9):646–656. https://doi.org/10.1038/s41560-020-0655-0
6. Ma N, Wu P, Wu Y, Jiang D, Lei G (2019) Progress and perspective of aqueous zinc-ion battery. Funct Mater Lett 12(05):1930003. https://doi.org/10.1142/s1793604719300032
7. Yu Y, Xie J, Zhang H, Qin R, Liu X, Lu X (2021) High-voltage rechargeable aqueous zinc-based batteries: latest progress and future perspectives. Small Sci 1(4):2000066. https://doi.org/10.1002/smsc.202000066
8. Yang C, Han M, Yan H, Li F, Shi M, Zhao L (2020) In-situ probing phase evolution and electrochemical mechanism of ZnMn2O4 nanoparticles anchored on porous carbon polyhedrons in high-performance aqueous Zn-ion batteries. J Power Sources 452:227826. https://doi.org/10.1016/j.jpowsour.2020.227826
9. Yang Q, Liang G, Guo Y, Liu Z, Yan B, Wang D, Huang Z, Li X, Fan J, Zhi C (2019) Do zinc dendrites exist in neutral zinc batteries: a developed electrohealing strategy to in situ rescue in-service batteries. Adv Mater 31(43):1903778. https://doi.org/10.1002/adma.201903778
10. Xie CL, Li YH, Wang Q, Sun D, Tang YG, Wang HY (2020) Issues and solutions toward zinc anode in aqueous zinc-ion batteries: a mini review. Carbon Energy 2(4):540–560. https://doi.org/10.1002/cey2.67
11. Dong N, Zhang F, Pan H (2022) Towards the practical application of Zn metal anodes for mild aqueous rechargeable Zn batteries. Chem Sci 13(28):8243–8252. https://doi.org/10.1039/d2sc01818g
12. Wang F, Borodin O, Gao T, Fan X, Sun W, Han F, Faraone A, Dura JA, Xu K, Wang C (2018) Highly reversible zinc metal anode for aqueous batteries. Nat Mater 17(6):543–549. https://doi.org/10.1038/s41563-018-0063-z
13. Lu W, Xie C, Zhang H, Li X (2018) Inhibition of zinc dendrite growth in zinc-based batteries. ChemSusChem 11(23):3996–4006. https://doi.org/10.1002/cssc.201801657
14. Li H, Ma L, Han C, Wang Z, Liu Z, Tang Z, Zhi C (2019) Advanced rechargeable zinc-based batteries: recent progress and future perspectives. Nano Energy 62:550–587. https://doi.org/10.1016/j.nanoen.2019.05.059
15. Zhang Q, Luan J, Tang Y, Ji X, Wang H (2020) Interfacial design of dendrite-free zinc anodes for aqueous zinc-ion batteries. Angewandte Chemie-Int Ed 59(32):13180–13191. https://doi.org/10.1002/anie.202000162
16. Zhao Z, Zhao J, Hu Z, Li J, Li J, Zhang Y, Wang C, Cui G (2019) Long-life and deeply rechargeable aqueous zn anodes enabled by multifunctional brightener-inspired interphase. Energy Environ Sci 12:1938–1949. https://doi.org/10.1039/C9EE00596J
17. Zhang Q, Luan J, Huang X, Wang Q, Sun D, Tang Y, Ji X, Wang H (2020) Revealing the role of crystal orientation of protective layers for stable zinc anode. Nat Commun 11(1):3961. https://doi.org/10.1038/s41467-020-17752-x
18. Yang H, Chang Z, Qiao Y, Deng H, Mu X, He P, Zhou H (2020) Constructing a super-saturated electrolyte front surface for stable rechargeable aqueous zinc batteries. Angewandte Chemie-Int Ed 59(24):9377–9381. https://doi.org/10.1002/anie.202001844
19. Zhang N, Huang S, Yuan Z, Zhu J, Zhao Z, Niu Z (2021) Direct self-assembly of MXene on Zn anodes for dendrite-free aqueous zinc-ion batteries. Angewandte Chemie-Int Ed 60(6):2861–2865. https://doi.org/10.1002/anie.202012322
20. Shin J, Lee J, Kim Y, Park Y, Kim M, Choi JW (2021) Highly reversible, grain-directed zinc deposition in aqueous zinc ion batteries. Adv Energy Mater 11(39). https://doi.org/10.1002/aenm.202100676
21. Zou P, Zhang R, Yao L, Qin J, Kisslinger K, Zhuang H, Xin HL (2021) Ultrahigh-rate and long-life zinc–metal anodes enabled by self-accelerated cation migration. Adv Energy Mater 11(31):2100982. https://doi.org/10.1002/aenm.202100982
22. Qiu H, Du X, Zhao J, Wang Y, Ju J, Chen Z, Hu Z, Yan D, Zhou X, Cui G (2019) Zinc anode-compatible in-situ solid electrolyte interphase via cation solvation modulation. Nat Commun 10(1):5374. https://doi.org/10.1038/s41467-019-13436-3
23. Cao L, Li D, Hu E, Xu J, Deng T, Ma L, Wang Y, Yang XQ, Wang C (2020) Solvation structure design for aqueous Zn metal batteries. J Am Chem Soc 142(51):21404–21409. https://doi.org/10.1021/jacs.0c09794
24. Hao J, Yuan L, Ye C, Chao D, Davey K, Guo Z, Qiao SZ (2021) Boosting zinc electrode reversibility in aqueous electrolytes by using low-cost antisolvents. Angewandte Chemie-Int Ed 60(13):7366–7375. https://doi.org/10.1002/anie.202016531
25. Zhang Q, Ma Y, Lu Y, Zhou X, Lin L, Li L, Yan Z, Zhao Q, Zhang K, Chen J (2021) Designing anion-type water-free Zn(2+) solvation structure for robust Zn metal anode. Angewandte Chemie-Int Ed 60(43):23357–23364. https://doi.org/10.1002/anie.202109682
26. Luo MH, Wang CY, Lu HT, Lu YH, Xu BB, Sun WP, Pan HG, Yan M, Jiang YZ (2021) Dendrite-free zinc anode enabled by zinc-chelating chemistry. Energy Storage Mater 41:515–521. https://doi.org/10.1016/j.ensm.2021.06.026
27. Cao J, Zhang D, Gu C, Zhang X, Okhawilai M, Wang S, Han J, Qin J, Huang Y (2021) Modulating Zn deposition via ceramic-cellulose separator with interfacial polarization effect for durable zinc anode. Nano Energy 89:106322. https://doi.org/10.1016/j.nanoen.2021.106322
28. Wang Y, Peng H, Hu M, Zhuang L, Lu J, Xiao L (2021) A stable zinc-based secondary battery realized by anion-exchange membrane as the separator. J Power Sources 486:229376. https://doi.org/10.1016/j.jpowsour.2020.229376
29. Yang H, Qiao Y, Chang Z, Deng H, He P, Zhou H (2020) A metal-organic framework as a multifunctional ionic sieve membrane for long-life aqueous zinc-iodide batteries. Adv Mater 32(38):2004240. https://doi.org/10.1002/adma.202004240
30. Ni Q, Kim B, Wu C, Kang K (2022) Non-electrode components for rechargeable aqueous zinc batteries: electrolytes, solid-electrolyte-interphase, current collectors, binders, and separators. Adv Mater 34(20):2108206. https://doi.org/10.1002/adma.202108206
31. Zhang Y, Li X, Fan L, Shuai Y, Zhang N (2022) Ultrathin and super-tough membrane for anti-dendrite separator in aqueous zinc-ion batteries. *Cell Reports Physical Science* 3(4):100824. https://doi.org/10.1016/j.xcrp.2022.100824
32. Liang Y, Wang Y, Mi H, Sun L, Ma D, Li H, He C, Zhang P (2021) Functionalized carbon nanofiber interlayer towards dendrite-free Zn-ion batteries. Chem Eng J 425:131862. https://doi.org/10.1016/j.cej.2021.131862
33. Li C, Sun Z, Yang T, Yu L, Wei N, Tian Z, Cai J, Lv J, Shao Y, Rummeli MH, Sun J, Liu Z (2020) Directly grown vertical graphene carpets as Janus separators toward stabilized Zn metal anodes. Adv Mater 32(33):2003425. https://doi.org/10.1002/adma.202003425
34. Chen M, Chen J, Zhou W, Han X, Yao Y, Wong CP (2021) Realizing an all-round hydrogel electrolyte toward environmentally adaptive dendrite-free aqueous Zn-MnO_2 batteries. Adv Mater 33(9):2007559. https://doi.org/10.1002/adma.202007559

35. Yufit V, Tariq F, Eastwood DS, Biton M, Wu B, Lee PD, Brandon NP (2019) Operando visualization and multi-scale tomography studies of dendrite formation and dissolution in zinc batteries. Joule 3(2):485–502. https://doi.org/10.1016/j.joule.2018.11.002
36. Qin Y, Liu P, Zhang Q, Wang Q, Sun D, Tang Y, Ren Y, Wang H (2020) Advanced filter membrane separator for aqueous zinc-ion batteries. Small 16(39):2003106. https://doi.org/10.1002/smll.202003106
37. Ghosh M, Vijayakumar V, Kurungot S (2019) Dendrite growth suppression by Zn^{2+}-integrated Nafion ionomer membranes: beyond porous separators toward aqueous Zn/V_2O_5 batteries with extended cycle life. Energ Technol 7(9):1900442. https://doi.org/10.1002/ente.201900442
38. Zheng J, Zhao Q, Tang T, Yin J, Quilty CD, Renderos GD, Liu X, Deng Y, Wang L, Bock DC, Jaye C, Zhang D, Takeuchi ES, Takeuchi KJ, Marschilok AC, Archer LA (2019) Reversible epitaxial electrodeposition of metals in battery anodes. Science 366(6465):645–648. https://doi.org/10.1126/science.aax6873
39. Wu B, Wang P, Yang H, Liang Y, Ni W, Xu G, Wei X, Yang L (2023) Design on modified glass fiber separator by graphite fluoride nanoflakes for Zn metal anodes with highly reversibility. J Power Sources 580:233323. https://doi.org/10.1016/j.jpowsour.2023.233323
40. Cao J, Zhang DD, Zhang XY, Sawangphruk M, Qin JQ, Liu RP (2020) A universal and facile approach to suppress dendrite formation for a Zn and Li metal anode. J Mater Chem A 8(18):9331–9344. https://doi.org/10.1039/d0ta02486d
41. An Y, Tian Y, Feng J, Qian Y (2022) MXenes for advanced separator in rechargeable batteries. Mater Today 57:146–179. https://doi.org/10.1016/j.mattod.2022.06.006
42. Liang Y, Ma D, Zhao N, Wang Y, Yang M, Ruan J, Yang G, Mi H, He C, Zhang P (2022) Novel concept of separator design: efficient ions transport modulator enabled by dual-interface engineering toward ultra-stable Zn metal anodes. Adv Funct Mater 32(25):2112936. https://doi.org/10.1002/adfm.202112936
43. Hou Z, Gao Y, Tan H, Zhang B (2021) Realizing high-power and high-capacity zinc/sodium metal anodes through interfacial chemistry regulation. Nat Commun 12(1):3083. https://doi.org/10.1038/s41467-021-23352-0
44. Su YW, Liu BZ, Zhang QH, Peng J, Wei CH, Li S, Li WP, Xue ZK, Yang XZ, Sun JY (2022) Printing-scalable Ti_3C_2Tx MXene-decorated janus separator with expedited Zn^{2+} flux toward stabilized Zn anodes. Adv Funct Mater 32(32):2204306. https://doi.org/10.1002/adfm.202204306
45. Zhang XT, Li JX, Qi KW, Yang YQ, Liu DY, Wang TQ, Liang SQ, Lu BA, Zhu YC, Zhou J (2022) An ion-sieving Janus separator toward planar electrodeposition for deeply rechargeable Zn-metal anodes. Adv Mater 34(38):2205175. https://doi.org/10.1002/adma.202205175
46. Liu TC, Hong J, Wang JL, Xu Y, Wang Y (2022) Uniform distribution of zinc ions achieved by functional supramolecules for stable zinc metal anode with long cycling lifespan. Energy Storage Mater 45:1074–1083. https://doi.org/10.1016/j.ensm.2021.11.002
47. Li S, Fu J, Miao G, Wang S, Zhao W, Wu Z, Zhang Y, Yang X (2021) Toward planar and dendrite-free Zn electrodepositions by regulating Sn-crystal textured surface. Adv Mater 33(21):2008424. https://doi.org/10.1002/adma.202008424
48. Fang Y, Lei P, Xing H, Xu K, Zhu M, Fan Z, Qi K, Wu Q, Zhu Y (2022) One-step targeted treatment for Zn flatting and protection. Energy Storage Mater 53:13–21. https://doi.org/10.1016/j.ensm.2022.08.045
49. Xu C-L, Li J-H, Feng Y-H, Yuan B, Liu J, Liu M, Shen F, Wang P-F, Han X (2022) Multifunctional hybrid interface enables controllable zinc deposition for aqueous Zn-ion batteries. J Power Sources 548:232044. https://doi.org/10.1016/j.jpowsour.2022.232044
50. Zou P, Chiang SW, Zhan H, Sui Y, Liu K, Hu S, Su S, Li J, Kang F, Yang C (2020) A periodic "self-correction" scheme for synchronizing lithium plating/stripping at ultrahigh cycling capacity. Adv Funct Mater 30(21):1910532. https://doi.org/10.1002/adfm.201910532
51. Liu H, Peng D, Xu T, Cai K, Sun K, Wang Z (2021) Porous conductive interlayer for dendrite-free lithium metal battery. J Energy Chem 53:412–418. https://doi.org/10.1016/j.jechem.2020.07.030
52. Pei A, Zheng G, Shi F, Li Y, Cui Y (2017) Nanoscale nucleation and growth of electrodeposited lithium metal. Nano Lett 17(2):1132–1139. https://doi.org/10.1021/acs.nanolett.6b04755
53. Dong G, Li S, Li T, Wu H, Nan T, Wang X, Liu H, Cheng Y, Zhou Y, Qu W, Zhao Y, Peng B, Wang Z, Hu Z, Luo Z, Ren W, Pennycook SJ, Li J, Sun J et al (2020) Periodic wrinkle-patterned single-crystalline ferroelectric oxide membranes with enhanced piezoelectricity. Adv Mater 32(50):2004477. https://doi.org/10.1002/adma.202004477
54. Zhang R, Chen XR, Chen X, Cheng XB, Zhang XQ, Yan C, Zhang Q (2017) Lithiophilic sites in doped graphene guide uniform lithium nucleation for dendrite-free lithium metal anodes. Angewandte Chemie-Int Ed 56(27):7764–7768. https://doi.org/10.1002/anie.201702099